polymers

MDPI

Article

Modification of NFA-Conjugated Bridges with Symmetric Structures for High-Efficiency Non-Fullerene PSCs

Qiuchen Lu [1], Ming Qiu [1], Meiyu Zhao [2,*], Zhuo Li [1] and Yuanzuo Li [1,*]

[1] College of Science, Northeast Forestry University, Harbin 150040, China; qiuchenlu1997@126.com (Q.L.); qm15765526850@163.com (M.Q.); 17733720476@163.com (Z.L.)

[2] School of Chemistry and Chemical Engineering, Harbin Institute of Technology, Harbin 150001, China

* Correspondence: myzhao@hit.edu.cn (M.Z.); yzli@nefu.edu.cn (Y.L.); Tel.: +86-451-8640-3305 (M.Z.); +86-451-8219-2245-8211 (Y.L.)

Received: 7 April 2019; Accepted: 10 May 2019; Published: 2 June 2019

Abstract: As electron acceptors, non-fullerene molecules can overcome the shortcomings of fullerenes and their derivatives (such as high cost, poor co-solubility, and weak light absorption). The photoelectric properties of two potential non-fullerene polymer solar cells (PSCs) PBDB-T:IF-TN (PB:IF) and PBDB-T:IDT-TN (PB:IDT) are studied by density functional theory (DFT) and time-dependent DFT (TD-DFT). Based on the optimized structure of the ground state, the effects of the electron donor (D) and electron acceptor (A) (D/A) interfaces PBDB-T/IF-TN (PB/IF) and PBDB-T/IDT-TN (PB/IDT) are studied by a quantum-chemical method (QM) and Marcus theory. Firstly, for two non-fullerene acceptors (NFAs) IF-TN and IDT-TN, the NFA IDT-TN has better optical absorption ability and better electron transport ability than IF-TN. Secondly, for the D/A interfaces PB/IF and PB/IDT, they both have high optical absorption and electron transfer abilities, and PB/IDT has better optical absorption and lower exciton binding energy. Finally, some important parameters (open-circuit voltage, voltage loss, fill factor, and power conversion efficiency) are calculated and simulated by establishing the theoretical model. From the above analysis, the results show that the non-fullerene PSC PB:IDT has better photoelectric characteristics than PB:IF.

Keywords: non-fullerene polymer solar cells; non-fullerene acceptor; small molecules; DFT; D/A interface; voltage loss; fill factor

1. Introduction

With the depletion of traditional fossil energy and serious environmental pollution, it is urgent to find new, clean, and sustainable energy. Solar energy is an excellent clean, sustainable, and new energy, and solar cells are important devices for the efficient collection and utilization of solar energy [1–6]. Among them, polymer solar cells (PSCs) have attracted wide attention because of their excellent properties, such as their small weights, low risk of pollution, high photoelectric conversion efficiencies (PCE), and the fact that they are easily manufactured on a large scale [7–10]. The energy conversion process of PSCs is divided into four basic steps [11,12]: (1) Sunlight excites the active layer molecules, and excitons are formed in the active layer; (2) the excitons are diffused to the interfaces of the electron donor (D) and the electron acceptor (A) (D/A interfaces); (3) the excitons undergo charge separation at the D/A interfaces, generating electrons and hole carriers; (4) charges are transferred to the electrodes to generate current. In order to convert light into electricity more effectively, the active layer molecules of PSCs should have characteristics well-matching with the sunlight spectrum, efficient charge transfer, the ability to produce many carriers, and lower loss of the carriers. The active layer, as an important part of the PSCs, is generally composed of electron donors and electron acceptors [13], which are

intermingled or formed into a bilayer structure. Fullerenes and their derivatives are the typical electron acceptors [14], and the PCE is over 10% for the PSCs of fullerenes and their derivatives [15]. However, the further development of fullerenes and their derivatives is limited by obvious defects, such as the high cost of manufacturing and purification, poor co-solubility with polymers, and weak absorption in visible and infrared bands. Some PSCs have overcome these shortcomings by using small molecules instead of fullerenes, which have displayed higher performance over fullerenes in comparative devices [16–20].

Non-fullerene small molecule electron acceptors have attracted increasing attention today because of their advantages, such as their easy synthesis, adjustable energy gaps, and high absorption coefficients [21–33]. Lin Y. et al. found that non-fullerene acceptors (NFAs) can be used as potential electron acceptors to replace fullerene acceptors (FAs) [21]. Li N. et al. found that in organic solar cells (OSCs) containing poly(3-hexylthiophen-2,5-diyl) (P3HT), the PCE could be increased from 2.8% to 6.05% by replacing the FAs phenyl-C_{61}-butyric acid methyl ester (PCBM) by the NFAs (5*Z*,5′*Z*)-5,5′-(((4,4,9,9-tetraoctyl-4,9-dihydro-*s*-indaceno[1,2-*b*:5,6-b′]dithiophene-2,7-diyl)bis(benzo[*c*]-[1,2,5]thiadiazole-7,4-diyl))bis-(methanylylidene))bis(3-ethyl-2-thioxothiazolidin-4-one)(O-IDTBR) [22]. Some excellent non-fullerene small electron acceptors have been reported [17–33], such as naphthalene diimide (NDI), perylene diimide (PDI), aromatic cores, and diketopyrrolopyrrole (DPP). The highest PCE for non-fullerene OSCs as non-fullerene small molecule acceptors for fused-ring electron acceptors has been over 15% [33].

Encouraged by a series of recent reports, we have investigated an electron-deficient acceptor unit, which is a novel moiety of 2-(3-oxo-2,3-dihydro-1H-cyclopenta [b]naphthalen-1-ylidene) malononitrile (N) connected to the end of the electron-donating core units. The electron-donating core units, indenofluorene (IF) and indacenodithiophene (IDT) can be used to form the NFAs IF-TN and IDT-TN (are shown in Figure 1) [34], where IDT can be made upon the replacement of the benzene ring in IF by thiophene. The geometric structures, and charge transport and photoelectric properties of the NFAs IF-TN, IDT-TN and donor polymer poly[(2,6-(4,8-bis(5-(2-ethylhexyl) thiophen-2-yl)benzo[1,2-*b*:4,5-*b*′]dithiophene)-co-(1,3-di(5-thiophene-2-yl)-5,7-bis(2-ethylhexyl)benzo [1,2-c:4,5-c′]dithiophene-4,8-dione)] (PBDB-T), and the charge transfer efficiencies at two interfaces PBDB-T/IF-TN (PB/IF) and PBDB-T/IDT-TN (PB/IDT) are studied by a quantum-chemical method (QM). The purpose of this work is to calculate and estimate the PCEs of two non-fullerene PSCs PBDB-T:IF-TN (PB:IF) and PBDB-T:IDT-TN (PB:IDT), by optimizing the geometrical structures of the NFAs IF-TN, IDT-TN, and PBDB-T, and constructing the interfaces at PB/IF and PB/IDT. We were able to obtain a series of photoelectric properties of the NFAs IF-TN and IDT-TN, and donor PBDB-T, such as HOMOs, LUMOs, ionization potentials (IPs), electron affinities (EAs), electrophilicity indexes (ω), electron and hole reorganization energies, absorption spectra, electron (hole) transport rates and mobilities, and the exciton separation rates at the PB/IF and PB/IDT interfaces. Open-circuit voltage (V_{OC}), voltage loss (V_{loss}), and fill factor (FF) are estimated by using molecular modeling.

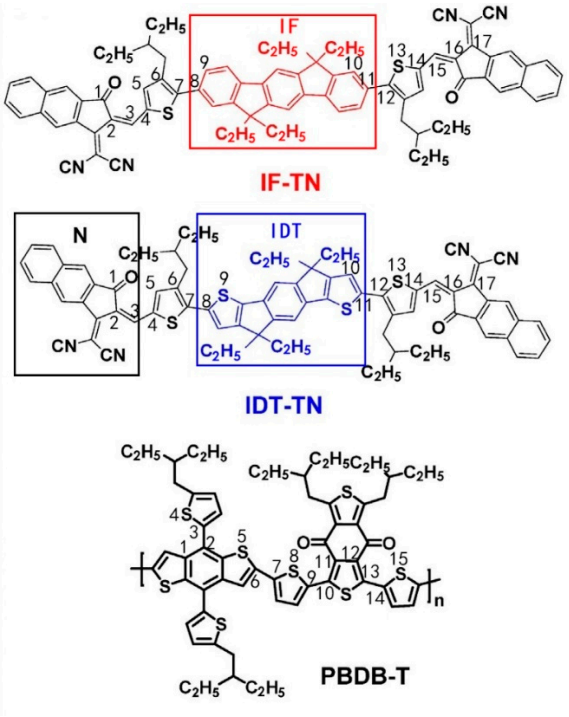

Figure 1. Molecular structure of the non-fullerene acceptors (NFAs) IF-TN, IDT-TN and donor PBDB-T.

2. Computational Methods

The ground state structures of the non-fullerene acceptors (NFAs) IF-TN and IDT-TN, and donor polymer PBDB-T (bond lengths, band angles, energy levels, ionization potentials (IPs), electron affinities (EAs), electrophilicity indexes, and reorganization energies) were optimized by using the density functional theory (DFT) [35] with B3LYP [36]/6-31G(d) method. The alkyl branches (R = C_4H_9&C_8H_{17}) on the small molecule chains were substituted by ethyl groups to save computing resources (the alkyl branch of the polymer has no significant effect on the optoelectronic properties [37]). The optical parameters of the small molecules were investigated using the time-dependent DFT (TD-DFT) [38] with CAM-B3LYP [39]/6-31G(d) method. All calculations were performed by using Gaussian09 suite [40]. The parameters (exchange integral, reorganization energy, and free enthalpy of the reaction) of the D/A interfaces (PB/IF and PB/IDT) were all investigated using the DFT/B3LYP/6-31G(d) method involved in Marcus theory. The exchange integrals of the D/A interfaces both adopted the finite field method [41] and the Generalized Mulliken–Hush (GMH) [42] model. The charge difference density (CDD) plots of the small molecules IF-TN, IDT-TN, and PBDB-T, as well as the D/A interfaces were visualized by using Multiwfn3.6 [43]. The parameters (transfer integrals) of the NFAs (IF-TN and IDT-TN) were all investigated by using the DFT/PW91PW91/6-31G(d) method involved in Marcus theory [44].

3. Results and Discussion

3.1. Geometric Structures

The chemical structures (bond lengths and angles) of the NFAs (IF-TN and IDT-TN) are shown in Table 1 and Figure 1 (the bond lengths and angles of the donor PBDB-T are shown in Table S1). The bond length of C_7–C_8 is 1.446 Å in NFA IDT-TN, and the bond length of C_7–C_8 is 1.472 Å in NFA IF-TN. The bond angle of C_6–C_7–C_8–S_9 is –21.92° in NFA IDT-TN, and the bond angle of C_6–C_7–C_8–C_9 is –50.72° in NFA IF-TN. It can be seen that when the benzene ring in the electron-donating IF core unit (the red box portion in Figure 1) of NFA IF-TN is replaced by thiophene to obtain the IDT (the blue box portion in Figure 1) of NFA IDT-TN, the bond lengths and the absolute values of the bond angles between thiophene and thiophene are decreased significantly compared to those between

thiophene and a benzene ring, which is due to the intermolecular repulsion between thiophene and thiophene. Improvement of the planarity of NFAs can effectively narrow the energy gap and broaden the optical absorption range of NFAs, which also effectively enhance the electron mobility of NFAs [45]. Furthermore, the donor polymer PBDB-T has a little degree of distortion (the largest dihedral angle is −56.31°).

Table 1. The bond lengths and bond angles for non-fullerene acceptor-based IF-TN and IDT-TN.

Length (Å)	**C_2-C_3**	**C_3-C_4**	**C_7-C_8**	**C_{11}-C_{12}**	**C_{14}-C_{15}**	**C_{15}-C_{16}**
IF-TN	1.380	1.425	1.472	1.471	1.424	1.380
IDT-TN	1.381	1.422	1.446	1.442	1.421	1.382
Angle (°)	C_1-C_2-C_3-C_4	C_2-C_3-C_4-C_5	C_6-C_7-C_8-C(S)$_9$	C_{10}-C_{11}-C_{12}-S_{13}	C_{13}-C_{14}-C_{15}-C_{16}	C_{14}-C_{15}-C_{16}-C_{17}
IF-TN	3.81	4.49	-50.72	43.79	176.38	−179.88
IDT-TN	2.95	3.49	−21.92	26.94	175.31	−179.36

At the same time, the aromaticity of IDT-TN has also been reduced upon substitution. Since the ionization potential (IP) of thiophene is lower than that of the benzene ring, the IP of NFA IDT-TN upon substitution has also been decreased. This can promote the separation of electrons from NFA IDT-TN, and when considering the relationship between the HOMO and the IP, the smaller energy gap of IDT-TN can be found.

The energy gaps, energy levels, and frontier molecular orbitals (FMOs) of the NFAs (IF-TN and IDT-TN) and donor polymer PBDB-T are shown in Figure 2 and Table S2. It can be seen that the HOMO levels of the NFAs IF-TN and IDT-TN, and donor PBDB-T are −5.579, −5.251, and −4.932 eV, respectively, while the LUMO levels are −3.193, −3.299, and −2.302 eV, respectively. The energy gaps ($\Delta_{H\text{-}L}$) are 2.386, 1.952, and 2.630 eV, respectively. It can be seen that the NFA IDT-TN has a lower energy gap than IF-TN, and the absorption peak of the NFA IDT-TN may have a wider absorption area and red-shift relative to IF-TN. Therefore, the non-fullerene PSC PB:IDT may have a higher J_{SC}, owing to absorbing more solar energy [46].

It can be seen from Figure 2 that the electron clouds of the HOMOs of the NFAs IF-TN and IDT-TN are more concentrated near the IF (the red box portion in Figure 1) and IDT (the blue box portion in Figure 1) regions. The LUMOs are more concentrated near the N (the black box portion in Figure 1) regions. This describes that the IF (or IDT) and N have stronger electron-withdrawing abilities and hole-withdrawing abilities, respectively, compared to other parts of the NFAs. However, the IDT-TN has a stronger electron-withdrawing ability relative to IF-TN because of the structure of the electron-donating core units. Therefore, the electrons are transferred from the N to the IF (or IDT) region when the NFAs are stimulated by sunlight, and among the two systems, the IDT-TN is the better NFA because the IDT region can attract more electrons.

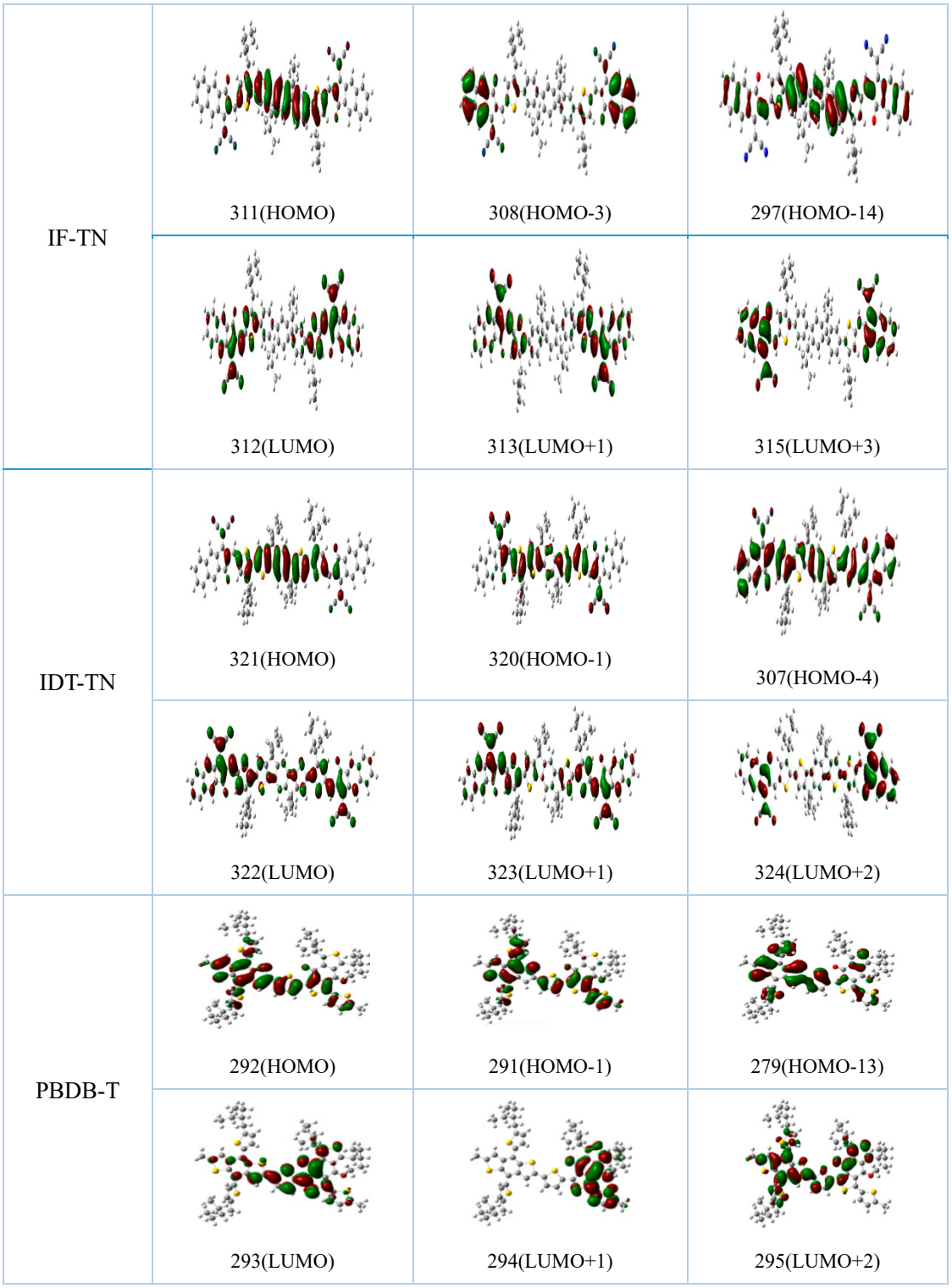

Figure 2. The frontier molecular orbital plots of the NFAs IF-TN and IDT-TN, and donor PBDB-T (where the red color represents electrons and green represents holes).

3.2. Ionization Potentials, Electron Affinities, and Reorganization Energies

Electron affinities (EAs) and ionization potentials (IPs) can be used to evaluate the degrees of difficulty of hole–electron binding and molecular ionization, respectively, which also represent the electron and hole barriers in the electron transport of the PSCs. Higher EAs and lower IPs can facilitate

the injection of electrons and the separation of excitons, respectively [47,48]. The EAs and IPs of the NFAs IF-TN and IDT-TN, and donor PBDB-T are shown in Table 2, in which the EAs of the NFAs IF-TN and IDT-TN, and donor PBDB-T are 2.533, 2.666, and 1.482 eV, respectively, and the IPs are 6.272, 5.912, and 5.702 eV, respectively. The NFA IDT-TN has a higher EA and lower IP relative to IF-TN. Therefore, the PSC PB:IDT has a better efficiency of electron injection and exciton separation.

Table 2. Ionization potentials, electron affinities, hardness, electrophilicity indexes, electro-accepting powers, and reorganization energies of the NFAs IF-TN and IDT-TN, and donor PBDB-T.

E (eV)	IF-TN	IDT-TN	PBDB-T
IP	6.272	5.912	5.702
EA	2.533	2.666	1.482
η	1.870	1.623	2.110
ω	5.184	5.667	3.057
ω^+	3.216	3.726	1.525
λ_h	0.196	0.214	0.247
λ_e	0.0906	0.136	0.266

The electrophilicity index (ω) can be used to evaluate the degree of electrophilic power. The results show that lower hardness (η) can lead to lower intramolecular charge transfer resistance, and that higher ω and electro-accepting power (ω^+) can lead to stronger electron-withdrawing ability [49].

The η values of the NFAs IF-TN and IDT-TN, and donor PBDB-T are 1.870, 1.623, and 2.110 eV, respectively, while the ω values are 5.184, 5.667, and 3.057 eV, respectively. The ω^+ values are 3.216, 3.726, and 1.525 eV, respectively. One can know that the NFA IDT-TN has the lower η, and higher ω and ω^+, showing that IDT-TN should have lower intramolecular charge transfer resistance and stronger electron-withdrawing power compared to IF-TN.

The reorganization energy (λ) can be used to evaluate the degree of charge transport characteristics of PSCs, and lower hole-reorganization energy (λ_h) can lead to a higher charge transfer rate [50–54]. The λ_h values of the NFAs IF-TN and IDT-TN, and donor PBDB-T are 0.196, 0.214, and 0.247 eV, respectively, while the λ_e values are 0.0906, 0.136, and 0.266 eV, respectively. Thus, IDT-TN may have the lower electron transport rate and electron mobility relative to IF-TN because of the higher λ_e.

3.3. Optical Absorption Properties

The active layer molecules absorbing solar energy are excited, causing them to produce excitons in the PSCs. The absorption spectra and excited-state lifetimes are important factors to measure the ability of an active layer to absorb solar energy. The transition energies, oscillator strengths (*f*), configuration interaction (CI) coefficients, and excited-state lifetimes (τ) for the NFAs IF-TN and IDT-TN, and donor PBDB-T are shown in Table 3 [55]. The absorption spectra and charge difference density (CDD) plots of the NFAs IF-TN and IDT-TN, and donor PBDB-T are shown in Figure 3a and Figure S1, respectively. At the same time, the transition energies, oscillator strengths, CI coefficients and light harvesting efficiency (LHE) of the interfaces PB/IF and PB/IDT are shown in Table S3 [56,57].

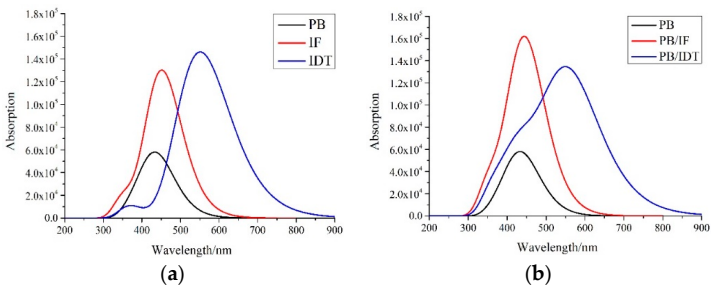

Figure 3. (**a**) The simulated absorption spectra of the NFAs IF-TN and IDT-TN, and donor PBDB-T. (**b**) The simulated absorption spectra of two interfaces (PB/IF and PB/IDT).

Table 3. Values for transition energy E (eV), absorption peak λ (nm), oscillator strength, configuration interaction (CI) coefficient and excited-state lifetime τ (ns) of the NFAs IF-TN, IDT-TN and donor PBDB-T.

Molecules	State	E	λ	Contribution MOs [a]	Strength f	τ
IF-TN	S1	2.7416	452.24	H→L (0.49617)	3.1814	0.964
	S2	2.8836	429.97	H→L+1 (0.45564)	0.0171	
	S3	3.4787	356.41	H-3→L+1 (0.38543)	0.4632	
	S4	3.4953	354.71	H-3→L (0.38995)	0.0084	
	S5	3.5148	352.75	H-14→L+3 (0.31064)	0.0278	
	S6	3.5173	352.50	H-13→L+1 (0.28640)	0.0141	
IDT-TN	S1	2.2474	551.69	H→L (0.58699)	3.5957	1.269
	S2	2.5793	480.69	H→L+1 (0.54405)	0.0258	
	S3	3.3436	370.81	H-1→L+1 (0.36306)	0.2604	
	S4	3.3676	368.17	H-1→L (0.36734)	0.0062	
	S5	3.4431	360.09	H→L+2 (0.36588)	0.0036	
	S6	3.4958	354.67	H-14→L+2 (0.25121)	0.0010	
PBDB-T	S1	2.8259	438.74	H→L (0.61234)	1.3271	2.174
	S2	3.2606	380.25	H→L+1 (0.48889)	0.3204	
	S3	3.5243	351.79	H-1→L (0.51487)	0.1427	
	S4	3.6137	343.10	H-14→L (0.23288)	0.0067	
	S5	3.6200	342.50	H-13→L+1 (0.45320)	0.0108	
	S6	3.8745	320.00	H→L+2 (0.46964)	0.1878	

[a]: H and L represent HOMO and LUMO, respectively.

The absorption spectra and charge difference density plots of the interfaces PB/IF and PB/IDT are shown in Figures 3b and 4, respectively. The light absorption of the active layer is a key parameter of PSCs, that is to say, a good active layer should have broad and strong absorption spectra relative to the solar spectra. The absorption peaks of S1 of the NFAs IF-TN and IDT-TN, and donor PBDB-T are 452.24, 551.69, and 438.74 nm, respectively. The oscillator strengths are 3.1814, 3.5957, and 1.3271, respectively. The excited-state lifetimes are 0.964, 1.269, and 2.174 ns, respectively.

As shown, for the NFAs IF-TN and IDT-TN, and donor PBDB-T, the strongest absorption state (where the oscillator strength f is largest) is the S1 excited state, which is the electron transfer from the HOMO to the LUMO level. The oscillator strength f of the S1 state and the excited-state lifetime τ are better for the NFA IDT-TN than for IF-TN. Therefore, IDT-TN has the obviously red-shifted absorption spectra and excitons staying in excited state for longer times. It can be seen from Figure 3a that the absorption peak of IDT-TN has an obvious red-shift relative to IF-TN, and IDT-TN also has the broader absorption spectra. The absorption peaks of S1 of the interfaces PB/IF and PB/IDT are 456.23 and 558.31 nm, respectively. The oscillator strengths are 2.1406 and 3.1576, respectively. The LHEs are 0.993 and 0.999, respectively. For the interfaces PB/IF and PB/IDT, the strongest absorption state is also the S1 excited state. Nevertheless, the electron transfers are from the HOMO-2 to LUMO levels or HOMO-1 to LUMO levels, respectively. The interface PB/IF has the larger oscillator strength f of the S1 state and LHE compared to PB/IF. It can be seen from Figure 3b that the interface PB/IDT has the obviously red-shifted absorption peak compared to PB/IF, and the PB/IDT also has the wider and stronger absorption spectra.

The charge difference densities (CDD) are analyzed and calculated in order to make the electron transfer processes of the NFAs and between donors and acceptors clearer and more intuitive [58]. As shown in Figure S1, for the NFAs IF-TN and IDT-TN, and donor PBDB-T, it can be seen that there are more electrons localized on the structures of electron-donating IDT core units of the NFA IDT-TN. For the interface PB/IF, it can be seen from Figure 4 that for the S1, S4, and S7 states, all electrons and holes are located on the NFA IF-TN. For the S2 and S6 states, all electrons and holes are located on the donor PBDB-T, while for the S3, S5, S8, and S9 states, electrons and holes are completely separated and distributed on the NFA and the donor, respectively. The S3 state is the minimum charge state, and the charges are completely separated at the PB/IF interface. When all electrons are located on the NFA IF-TN, the electrons are mainly located on the structures of electron-donating IF core units. For the

PB/IDT interfaces, it can also be seen from Figure 4 that for the S1, S2, S7, and S9 states, all electrons and holes are located on the NFA IDT-TN. For the S4 and S6 states, all electrons and holes are located on the donor PBDB-T, while for the S3, S5, and S8 states, electrons and holes are completely separated and distributed on the NFA and the donor, respectively. The S3 state is viewed as the minimum charge state, and the charges are completely separated at the PB/IDT interface. When all electrons are located on the NFA IDT-TN, the electrons are mainly located on the structures of electron-donating IDT core units. Thus, it can be seen that the strongest absorption states are the S1 excited states for both PB:IF and PB:IDT active layers, and that the NFAs play key roles in absorbing sunlight.

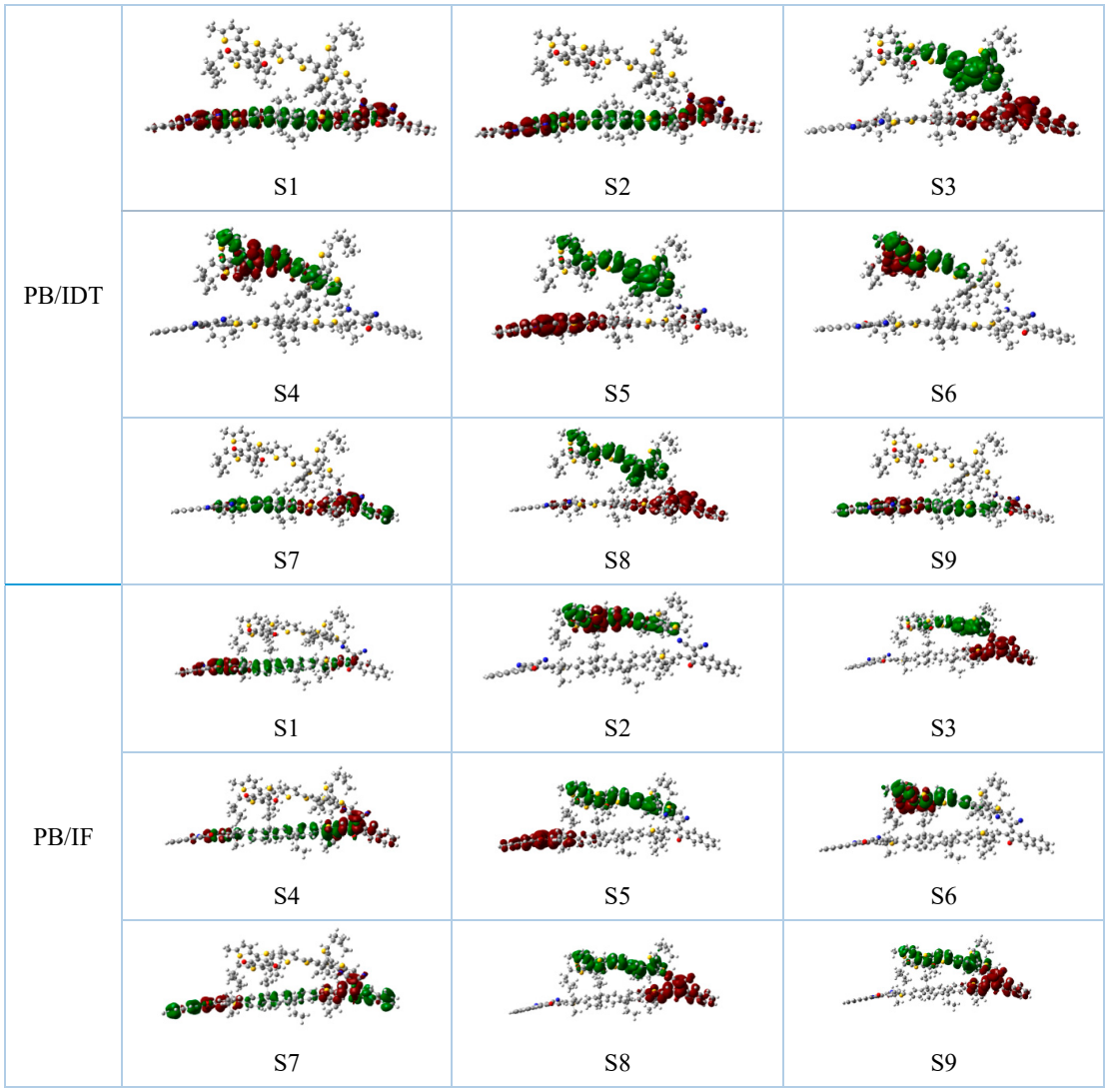

Figure 4. The representative charge difference density plots of two interfaces (PB/IF and PB/IDT) (red represents electrons, green represents holes).

3.4. The Excitons Separation Rate at the D/A Interfaces in Marcus Theory

After excitons are generated in the active layer, they diffuse to the D/A interfaces and separate to form free electrons and hole carriers at the D/A interfaces [59–61]. The excitons separation rate is an important factor to measure the efficiency of excitons separation at the D/A interfaces. The Marcus theory is used to estimate the excitons separation rate at D/A interfaces [44,62]:

$$k_{CT} = \frac{|V_{DA}|^2}{\hbar}\sqrt{\frac{\pi}{\lambda k_B T}}\exp\left(\frac{-(\Delta G_{CT}+\lambda)^2}{4\lambda k_B T}\right) \quad (1)$$

where k_{CT}, V_{DA}, h, λ, k_B, T, and ΔG_{CT} are represented as the excitons separation rate, charge transfer integration [16,41,63–65] (i.e., difference of the electrons coupling matrix element between the initial and final states), the Planck constant, reorganization energy [66–68], the Boltzmann constant, temperature (we supposed that T is 300 K at room temperature), and free energy change of the excitons [69] separation reaction, respectively, and the above calculation process is listed in the supporting materials. V_{DA} can be calculated from Equations (S8) and (S9), λ can be calculated from Equations (S10) and (S11), and ΔG_{CT} can be calculated from Equation (S12).

From Equation (S12), the exciton binding energies (E_b) play an important role in the charge separation at the D/A interfaces in the PSCs, and the exciton binding energies (E_b) approximately equal to the coulomb interaction energy (E_{coul}) between the donor polymer and the NFAs during charge transfer [12,16,68]. The E_b is also approximately equal to the difference between the optical band gap and the electrochemical band gap (the electrochemical band gap can be the difference between the HOMO and LUMO levels of the D/A interfaces, and the value is generally between 0.2 and 1 eV) [12,16,65]:

$$E_b = |HOMO - LUMO| - E_{opt} \quad (2)$$

where HOMO, LUMO, and E_{opt} refer to the HOMO of the interfaces, the LUMO of the interfaces, and the optical band gap that can be approximated as the first excited energy of the donor polymer.

In the PSCs, the exciton binding energy and recombination energy should be as small as possible, and the charge transfer integration should be as large as possible. Under these conditions, the exciton separation rate can be as large as possible, meaning that the efficiency of producing the free electrons and hole carriers is further improved when the charge separation occurs at D/A interfaces. The E_b, V_{DA}, λ, ΔG_{CT}, and k_{CT} are shown in Table 4, and the k_{CT1} and k_{CT2} of the D/A interfaces PB/IF and PB/IDT can be seen in Figure 5.

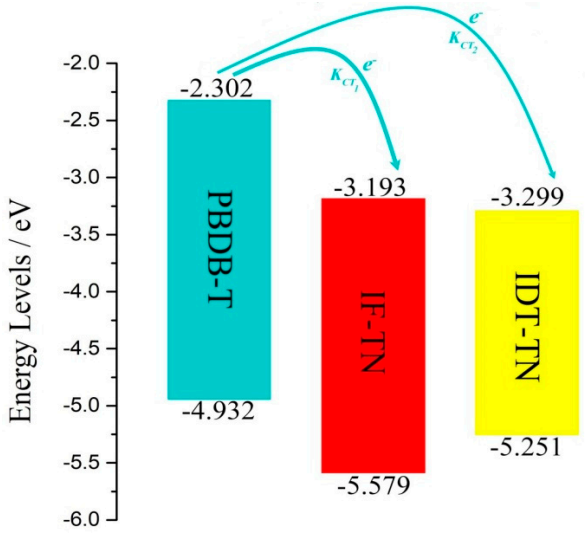

Figure 5. Energy levels of the NFAs IF-TN and IDT-TN and donor PBDB-T, and the charge transfer at the two interfaces (PB/IF and PB/IDT).

Table 4. Calculated exciton binding energy E_b (eV), charge transfer integral V_{DA} (eV), reorganization energy λ (eV), Gibbs free energy change ΔG_{CT} (eV) and excitons separation rate k_{CT} (s^{-1}) of two interfaces (PB/IF and PB/IDT).

Interfaces	E_b	V_{DA}	λ	ΔG_{CT}	k_{CT}
PB/IDT	0.631	0.184	0.505	−0.421	6.972×10^{14}
PB/IF	0.970	0.316	0.478	−0.628	1.538×10^{15}

It can be seen that the E_b values of the interfaces PB/IF and PB/IDT are 0.970 and 0.631 eV, respectively. The V_{DA} values are 0.316 and 0.184 eV, respectively, and the λ values are 0.478 and 0.505 eV, respectively. The ΔG_{CT} values are −0.628 and −0.421 eV, respectively, while the k_{CT} values of the interfaces are 1.538×10^{15} and 6.972×10^{14} s^{-1}, respectively. As shown, the interface PB/IDT has a relatively smaller k_{CT} relative to PB/IF because of the lower V_{DA} and larger λ. At the same time, it can also be found that the interface PB/IDT has a larger difference between the LUMO of the donor polymer and the LUMO of IDT-TN (L_D–L_A), because IDT-TN has the lower LUMO (as can be seen in Figure 5). Furthermore, the D/A interface PB/IDT has the lower E_b value, which has positive influence on the behavior of the D/A interface.

3.5. Electron Transport Rate and Mobility of NFAs

After the excitons are separated at the interface to produce free electrons and hole carriers, the free electrons and hole carriers diffuse to the NFAs phase and donor polymer phase, respectively [45]. The electron transport rate and mobility are the key factors to measure the transport efficiency of free electrons in the NFAs phase. Higher electron transport rate and mobility of the NFAs can lead to having higher electron transport efficiency, and the PSCs can also have a higher short-circuit current (J_{SC}). The transport of electrons in organic semiconductors is usually considered to be an incoherent transition process under the weak interaction of molecules at room temperature (T = 300 K), and in the discontinuous transition process, electrons are usually considered to migrate through the NFAs by jumping between adjacent molecules. Marcus theory is usually used to estimate the electron mobility of the NFAs when the temperature is high enough [44,62]:

$$\mathrm{k} = \frac{t^2}{\hbar}\sqrt{\frac{\pi}{\lambda k_B T}}\exp\left(\frac{-\lambda^2}{4k_B T}\right) \tag{3}$$

where λ, t, T, and k_B represent the reorganization energy, charge transfer integral, room temperature (300 K), and the Boltzmann constant, respectively. According to Kupman's theorem, in the electron transport reaction of an anionic system (electron transport) and the electron transport reaction of a cationic system (hole transport), the charge transfer integrals can be approximately considered as half of the difference of energy between the LUMO + 1 and LUMO of two adjacent neutral systems [70,71]:

$$t_e = \frac{E_{LUMO+1} - E_{LUMO}}{2} \tag{4}$$

As the acceptor materials of the active layer in the PSCs (electron transport layer), the NFAs should have good electron transport ability, and as the donor materials of the active layer in the PSCs (hole transport layer), the donor polymers should have good hole transport ability. A high electron transport rate of the NFAs should lead to high electron mobility, which indicates that the NFAs should have high electron transport ability and should have great potential as good electron transport materials.

According to the Einstein equation, electron mobility can be calculated as [72,73]:

$$\mu = \frac{e}{k_B T}D \tag{5}$$

where k_B represents the Boltzmann constant, T represents room temperature (300 K), e represents electron charge, and D represents the diffusion coefficient. When electrons are migrated by means of jumping along with a particular path (one-dimensional), electron mobility can be calculated as [73–75]:

$$\mu = \frac{er^2}{2k_B T}k \tag{6}$$

where r and K are the jumping distance between adjacent molecules and the charge transfer rate, respectively. The electron transfer integral t_e, electron reorganization energy λ_e, electron transport rate

k_e, electron diffusion constant D_e, and the electron mobility μ_e of the NFAs IF-TN and IDT-TN are shown in Table 5. The hole transfer integral t_h, hole reorganization energy λ_h, hole transport rate k_h, hole diffusion constant D_h, and the hole mobility μ_h of the NFAs IF-TN and IDT-TN can be seen in Table S4.

Table 5. Calculated electron transfer integral t_e (eV), electron reorganization energy λ_e (eV), electron transport rate k_e (s^{-1}), distance r (Å), electron diffusion constant D_e (cm^2/s), and the electron mobility μ_e ($cm^2/(V \cdot s)$) of the NFAs IF-TN and IDT-TN.

Dimers	t_e	λ_e	k_e	r	D_e	μ_e
IF-TN	0.00395	0.0906	3.607×10^{12}	4.8824	4.299×10^{-4}	0.0166
IDT-TN	0.00898	0.136	9.822×10^{11}	4.8287	1.145×10^{-3}	0.0443

As shown in Table 5, the electron transfer integral t_e, electron reorganization energy λ_e, electron transport rate k_e, electron diffusion constant D_e, and the electron mobility μ_e of the NFA IF-TN are 0.00395 eV, 0.0906 eV, 3.607×10^{12} s^{-1}, 4.299×10^{-4} cm^2/s, and 0.0166 $cm^2/(V \cdot s)$, respectively. The electron transfer integral t_e, electron reorganization energy λ_e, electron transport rate k_e, electron diffusion constant D_e, and electron mobility μ_e of the NFA IDT-TN are 0.00898 eV, 0.136 eV, 9.822×10^{11} s^{-1}, 1.145×10^{-3} cm^2/s, and 0.0443 $cm^2/(V \cdot s)$, respectively. It can be seen that the NFA IDT-TN has a higher μ_e because of the larger t_e. The value of μ_e for the NFA IDT-TN is about three times that of the NFA IF-TN, which means that IDT-TN is the better electron transport material compared to IF-TN.

According to the structures of the NFAs IF-TN and IDT-TN, one of the reasons why the NFA IDT-TN has the larger electron mobility (μ_e) is the fact that the aromaticity of IDT-TN is reduced, and the electron transfer integral is increased, which promotes the free movement of electrons intermolecular. The PSC PB:IDT may have a higher short-circuit current (J_{SC}).

3.6. Macroscopic Properties of Non-Fullerene PSCs

It is well known that the open-circuit voltage (V_{OC}), fill factor (FF), and power conversion efficiency (PCE) are all very important parameters for evaluating the macroscopic properties of non-fullerene PSCs. The V_{OC} values of the PSCs can be approximately considered to be in direct proportion to the absolute values of the differences between HOMOs of donor polymer and LUMOs of the NFAs [76], and the NFAs with the higher LUMO levels have higher V_{OC} values. In theory, Equation (7) is used to estimate the V_{OC} of the PSCs [77].

$$V_{OC} = \frac{1}{e}(E_{HOMO}(D) - E_{LUMO}(A)) - \Delta V \quad (7)$$

where E_{HOMO} (D), E_{LUMO} (A), e, and ΔV are represented as the HOMO level of the donor polymer, the LUMO levels of the NFAs, the elemental charge, and the empirical constant (usually considered to be 0.3 V [78]), respectively. The fill factor (FF) is an important parameter for describing the photoelectric properties of the PSCs and calculating the PCE, and the fill factor in an ideal state FF_0 (ignoring the effects of parallel resistance and series resistance) can be calculated as [79,80]:

$$FF_0 = \frac{v_{oc} - \ln(v_{oc} + 0.72)}{v_{oc} + 1} \quad (8)$$

where the V_{OC} (V_{OC} is normalized to the thermal voltage) can be expressed by Equation (S15) [79,80], and the voltage loss (V_{loss}) can be expressed by Equation (S16) [81]. The energy gaps (E_g) of the donor, optical bandgaps (E_g) of the active layers, differences between the LUMOs of donor polymers and the LUMOs of the NFAs (L_D–L_A), V_{OC}, V_{loss}, and the fill factors in the ideal state (FF_0) of the PSCs PB:IF and PB:IDT are shown in Table 6.

Table 6. Calculated energy gaps E_g of donor (eV), optical bandgap E_g of the active layer (eV), difference between the HOMO of the donor and the LUMO of the acceptor H_D–L_A (eV), difference between the LUMO of the donor and the LUMO of the acceptor L_D–L_A (eV), the open-circuit voltage V_{OC} (V), voltage loss V_{loss} (V), and fill factor in the ideal state FF_0 (%) of two polymer solar cells (PSCs) (PB:IF and PB:IDT).

Cells	E_g	E_g	H_D-L_A	L_D-L_A	V_{OC}	V_{loss}	ν_{oc}	FF_0
PB:IF	2.631	2.718	1.739	0.563	1.439	1.279	55.663	91.12
PB:IDT	2.631	2.221	1.633	0.669	1.333	0.888	51.563	90.57

The E_g, E_g, L_D–L_A, V_{OC}, V_{loss}, and FF_0 values of the PSC PB:IF are 2.631 eV, 2.718 eV, 0.563 eV, 1.439 V, 1.279 V, and 91.12%, respectively. The E_g, E_g, L_D–L_A, V_{OC}, V_{loss}, and FF_0 values of the PSC PB:IDT are 2.631 eV, 2.221 eV, 0.669 eV, 1.333 V, 0.888 V, and 90.57%, respectively. As shown, the PSC PB:IDT has the relatively smaller V_{OC} and FF_0, but the differences of the V_{OC} and FF_0 values between the two NFAs are little. The PSC PB:IDT has a significantly lower V_{loss}, which may lead to improvement of the V_{OC} quality. The PSC PB:IDT also has a significantly higher μ_e, which may lead to improvement of the FF_0 [82].

For the power conversion efficiency (PCE), the Scharber diagram (by the contour lines and colors) is used to estimate the specific value of the PCE [83,84]. The Scharber diagram can be seen in Figure 6, and the PCE values of the PSCs PB:IF and PB:IDT are both 3%. Although the PSC PB:IF may have a higher V_{OC} and FF_0, the PSC PB:IDT has the wider, stronger, and more red-shifted absorption spectra, larger LHE, longer excited-state lifetime, higher voltage loss, and larger electron mobility. It is hoped that on the same order of magnitude for V_{OC} and FF_0, the PSC based on PB:IDT has the bigger external quantum efficiency (EQE) and short-circuit current (J_{SC}), which should lead to a better PCE.

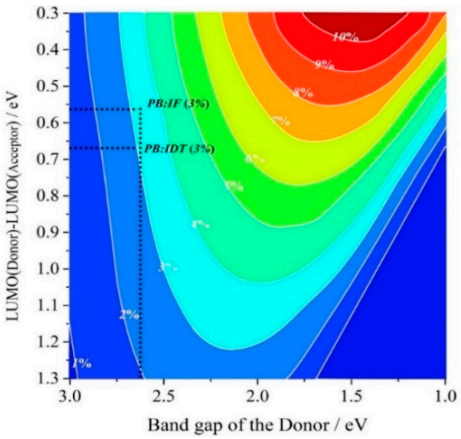

Figure 6. Predicted power conversion efficiency (PCE) for the PSCs PB:IF and PB:IDT with the Scharber diagram.

3.7. Built-In Electric Field Effect on the Optical Character

Built-in electric fields have effects on the optical properties of the donor polymers and NFAs by affecting the internal photochemistry of the PSCs [85,86]. The optical properties of the PSC PB:IDT under different built-in electric fields are calculated and analyzed to study the effects of built-in electric fields on the optical properties of PSC PB:IDT. The optical characters and absorption spectra of PSC PB:IDT under different built-in electric fields can be seen in Table 7 and Figure S2, respectively. The oscillators of the S1 state (where the oscillator strength f is the largest) of PSC PB:IDT are 3.1576, 3.1344, 3.0767, and 3.0007, respectively, and the absorption peaks are at 558.31, 558.48, 559.76, and 561.95 nm, respectively.

Table 7. Built-in electric field effects on optical character of the PSC PB:IDT.

Field ($\times 10^{-4}$ a.u.)	Peak of S1/nm	Engrgy/eV	Contribution Mos [a]	Strength *f*
0	558.31	2.221	H-1→L (0.53767)	3.1576
10	558.48	2.220	H→L (0.50854)	3.1344
20	559.76	2.215	H→L (0.49961)	3.0767
30	561.95	2.206	H→L (0.49280)	3.0007

[a]: H and L represent HOMO and LUMO, respectively.

Under the electric fields of 0, 10×10^{-4}, 20×10^{-4}, and 30×10^{-4} a.u., the absorption spectra of the PSC PB:IDT have gradually red-shifted (red-shift increments were 0.17, 1.45, and 3.64 nm under the built-in electric fields of energy intensity 0, 10×10^{-4}, 20×10^{-4}, and 30×10^{-4}, respectively, relative to the PSC PB:IDT without any built-in electric field), and the gene-base for oscillator strengths is increased. This result illustrates that the built-in electric fields have significant effects on the photoelectric properties of the PSC PB:IDT, and the appropriate increase of built-in electric fields may be helpful to improve the optical absorption effects of the PSC PB:IDT.

4. Conclusions

In this paper, the photoelectric performances of two non-fullerene PSCs were calculated to investigate and compare the two NFAs' (IF-TN and IDT-TN) abilities by the density functional theory (DFT) and time-dependent density functional theory (TD-DFT). At the same time, the structures and properties of the D/A interfaces PB/IF and PB/IDT were simulated by a quantum-chemical method (QM) and Marcus theory. The results show that: (a) For the NFAs IF-TN and IDT-TN, the NFA IDT-TN has the narrower energy gap, lower IPs, higher EAs, a larger electrophilicity index ω, a longer excited-state lifetime τ, larger absorption peaks, better planarity, a greater electron transport rate k_e, and greater mobility μ_e; (b) for the D/A interfaces PB/IF and PB/IDT, the D/A interface PB/IDT has the stronger and more red-shifted absorption spectra, bigger LHE, a smaller exciton binding energy E_b, and a slightly smaller excitons separation rate with little difference in value compared to that of PB/IF; (c) for the macro-photoelectric performance of non-fullerene PSCs (PB:IF and PB:IDT), the non-fullerene PSC PB:IDT has the lower voltage loss V_{loss}, and the slightly smaller open-circuit voltage V_{OC} and fill factor FF_0 with little differences in values compared to those of PB:IF, but however, the Jsc for the PB:IDT system has been significantly increased by substitution. It can be predicted that the PCEs of the non-fullerene PSCs (PB:IF and PB:IDT) can both reach 3% (and the PB:IDT should have a higher PCE). Finally, we can infer that the non-fullerene PSC PB:IDT should have more potential applications in solar cells.

Supplementary Materials: The following are available online at http://www.mdpi.com/2073-4360/11/6/958/s1.

Author Contributions: Conceptualization: Y.L. and M.Z.; Funding acquisition: Y.L.; Investigation and data analysis: Q.L. M.Q. and Z.L.; Software: Y.L. and M.Z.; Writing—original draft: Q.L.; Writing—review & editing: Q.L., M.Q. and Y.L.

Funding: This research was funded by the Fundamental Research Funds for the China Postdoctoral Science Foundation (2016M590270), the Central Universities (2572018BC24), Heilongjiang Postdoctoral Grant (LBH-Z15002), the National Natural Science Foundation of China (Grant Nos. 11404055 and 11374353), and college student research training program (KY2018018 and KY2018017).

Acknowledgments: This work was supported by the Fundamental Research Funds for the China Postdoctoral Science Foundation (2016M590270), the Central Universities (2572018BC24), Heilongjiang Postdoctoral Grant (LBH-Z15002), the National Natural Science Foundation of China (Grant Nos. 11404055 and 11374353), and college student research training program (KY2018018 and KY2018017).

Conflicts of Interest: The authors declare no conflict of interest.

References

1. Roes, A.L.; Alsema, E.A.; Blok, K.; Patel, M.K. Ex-ante environmental and economic evaluation of polymer photovoltaics. *Prog. Photovolt.* **2009**, *17*, 372–393. [CrossRef]
2. Chu, S.; Cui, Y.; Liu, N. The path towards sustainable energy. *Nat. Mater.* **2017**, *16*, 16–22. [CrossRef] [PubMed]
3. Chen, S.S.; Zhang, L.; Ma, C.; Meng, D.; Zhang, J.Q.; Zhang, G.Y.; Li, Z.K.; Chow, P.C.Y.; Ma, W.; Wang, Z.H.; et al. Alkyl chain regiochemistry of benzotriazole-based donor polymers influencing morphology and performances of non-fullerene organic solar cells. *Adv. Energy Mater.* **2018**, *8*, 6. [CrossRef]
4. Huo, Y.; Zhu, J.S.; Wang, X.Z.; Yan, C.Q.; Chai, Y.F.; Chen, Z.Z.; Zhan, X.W.; Zhang, H.L. Small molecule donors based on benzodithiophene and diketopyrrolopyrrole compatible with both fullerene and non-fullerene acceptors. *J. Mater. Chem. C* **2018**, *6*, 5843–5848. [CrossRef]
5. Zhang, W.; Hu, R.; Zeng, X.; Su, X.; Chen, Z.; Zou, X.; Peng, J.; Zhang, C.; Yartsev, A. Effect of post-thermal annealing on the performance and charge photogeneration dynamics of PffBT4T-2OD/PC_{71}BM solar cells. *Polymers* **2019**, *11*, 408. [CrossRef]
6. Li, W.; Cai, J.; Cai, F.; Yan, Y.; Yi, H.; Gurney, R.S.; Liu, D.; Iraqi, A.; Wang, T. Achieving over 11% power conversion efficiency in PffBT4T-2OD-based ternary polymer solar cells with enhanced open-circuit-voltage and suppressed charge recombination. *Nano Energy* **2018**, *44*, 155–163. [CrossRef]
7. Friend, R.H.; Gymer, R.W.; Holmes, A.B.; Burroughes, J.H.; Marks, R.N.; Taliani, C.; Bradley, D.D.C.; Santos, D.A.D.; Brédas, J L.; Lögdlund, M. Electroluminescence in conjugated polymers. *Nature* **1999**, *397*, 121–128. [CrossRef]
8. He, B.; Li, Z.; Jia, T.; Xin, J.; Ying, L.; Ma, W.; Huang, F.; Cao, Y. Star-like n-type conjugated polymers based on naphthalenediimide for all-polymer solar cells. *Dyes Pigment.* **2018**, *159*, 85–91. [CrossRef]
9. Cheng, P.; Zhan, X. Stability of organic solar cells: Challenges and strategies. *Chem. Soc. Rev.* **2016**, *45*, 2544–2582. [CrossRef]
10. Ye, L.; Zhang, S.; Huo, L.; Zhang, M.; Hou, J. Molecular design toward highly efficient photovoltaic polymers based on two-dimensional conjugated benzodithiophene. *Acc. Chem. Res.* **2014**, *47*, 1595–1603. [CrossRef]
11. Ye, L.; Jiao, X.; Zhou, M.; Zhang, S.; Yao, H.; Zhao, W.; Xia, A.; Ade, H.; Hou, J. Manipulating aggregation and molecular orientation in all-polymer photovoltaic cells. *Adv. Mater.* **2015**, *27*, 6046–6054. [CrossRef]
12. Li, Y.; Pullerits, T.; Zhao, M.; Sun, M. Theoretical characterization of the PC60BM:PDDTT model for an organic solar cell. *J. Phys. Chem. C* **2011**, *115*, 21865–21873. [CrossRef]
13. Cheng, P.; Li, G.; Zhan, X.; Yang, Y. Next-generation organic photovoltaics based on non-fullerene acceptors. *Nat. Photon.* **2018**, *12*, 131–142. [CrossRef]
14. Ray, A.; Bhattacharya, S. Photophysical insights behind zinc naphthalocyanine-gold nanoparticle interaction and its effect over supramolecular interaction between zinc napthalocyanine and PyC60 in solution. *J. Mol. Liq.* **2017**, *232*, 188–194. [CrossRef]
15. Liu, T.; Pan, X.X.; Meng, X.Y.; Liu, Y.; Wei, D.H.; Ma, W.; Huo, L.J.; Sun, X.B.; Lee, T.H.; Huang, M.; et al. Alkyl Side-chain engineering in wide-bandgap copolymers leading to power conversion efficiencies over 10%. *Adv. Mater.* **2017**, *29*, 7. [CrossRef]
16. Wang, Q.; Li, Y.; Song, P.; Su, R.; Ma, F.; Yang, Y. Non-fullerene acceptor-based solar cells: From structural design to interface charge separation and charge transport. *Polymers* **2017**, *9*, 692. [CrossRef]
17. Liu, Z.; Wu, Y.; Zhang, Q.; Gao, X. Non-fullerene small molecule acceptors based on perylene diimides. *J. Mater. Chem. A* **2016**, *4*, 17604–17622. [CrossRef]
18. Liu, Z.; Gao, Y.; Dong, J.; Yang, M.; Liu, M.; Zhang, Y.; Wen, J.; Ma, H.; Gao, X.; Chen, W.; et al. Chlorinated wide-bandgap donor polymer enabling annealing free nonfullerene solar cells with the efficiency of 11.5%. *J. Phys. Chem. Lett.* **2018**, *9*, 6955–6962. [CrossRef]
19. Ye, L.; Xiong, Y.; Chen, Z.; Zhang, Q.; Fei, Z.; Henry, R.; Heeney, M.; O'Connor, B.T.; You, W.; Ade, H. Sequential deposition of organic films with eco-compatible solvents improves performance and enables over 12%-efficiency nonfullerene solar cells. *Adv. Mater.* **2019**, *31*, 1808153. [CrossRef]
20. Ye, L.; Zhao, W.; Li, S.; Mukherjee, S.; Carpenter, J.H.; Awartani, O.; Jiao, X.; Hou, J.; Ade, H. High-efficiency nonfullerene organic solar cells: Critical factors that affect complex multi-length scale morphology and device performance. *Adv. Energy Mater.* **2017**, *7*, 1602000. [CrossRef]

21. Lin, Y.; Zhan, X. Non-fullerene acceptors for organic photovoltaics: An emerging horizon. *Mater. Horizons* **2014**, *1*, 470–488. [CrossRef]
22. Li, N.; McCulloch, I.; Brabec, C.J. Analyzing the efficiency, stability and cost potential for fullerene-free organic photovoltaics in one figure of merit. *Energy Environ. Sci.* **2018**, *11*, 1355–1361. [CrossRef]
23. Zhang, Y.M.; Kan, B.; Sun, Y.N.; Wang, Y.B.; Xia, R.X.; Ke, X.; Yi, Y.Q.Q.; Li, C.X.; Yip, H.L.; Wan, X.J.; et al. Nonfullerene Tandem organic solar cells with high performance of 14.11%. *Adv. Mater.* **2018**, *30*, 7. [CrossRef]
24. Lin, Y.; Zhao, F.; He, Q.; Huo, L.; Wu, Y.; Parker, T.C.; Ma, W.; Sun, Y.; Wang, C.; Zhu, D. High-performance electron acceptor with thienyl side chains for organic photovoltaics. *J. Am. Chem. Soc.* **2016**, *138*, 4955–4961. [CrossRef] [PubMed]
25. Zheng, Z.; Zhang, S.; Zhang, J.; Qin, Y.; Li, W.; Yu, R.; Wei, Z.; Hou, J. Over 11% efficiency in tandem polymer solar cells featured by a low-band-gap polymer with fine-tuned properties. *Adv. Mater.* **2016**, *28*, 5133–5138. [CrossRef] [PubMed]
26. Meng, D.; Fu, H.; Xiao, C.; Meng, X.; Winands, T.; Ma, W.; Wei, W.; Fan, B.; Huo, L.; Doltsinis, N.L. Three-bladed rylene propellers with three-dimensional network assembly for organic electronics. *J. Am. Chem. Soc.* **2016**, *138*, 10184–10190. [CrossRef]
27. Anthony, J.E. Small-molecule, nonfullerene acceptors for polymer bulk heterojunction organic photovoltaics. *Chem. Mater.* **2011**, *23*, 583–590. [CrossRef]
28. Eftaiha, A.F.; Sun, J.P.; Hill, I.G.; Welch, G.C. Recent advances of non-fullerene, small molecular acceptors for solution processed bulk heterojunction solar cells. *J. Mater. Chem. A* **2014**, *2*, 1201–1213. [CrossRef]
29. Holliday, S.; Ashraf, R.S.; Nielsen, C.B.; Kirkus, M.; Rohr, J.A.; Tan, C.H.; Collado-Fregoso, E.; Knall, A.C.; Durrant, J.R.; Nelson, J. A rhodanine flanked nonfullerene acceptor for solution-processed organic photovoltaics. *J. Am. Chem. Soc.* **2015**, *137*, 898–904. [CrossRef]
30. Zhong, Y.; Trinh, M.T.; Chen, R.S.; Wang, W.; Khlyabich, P.P.; Kumar, B.; Xu, Q.Z.; Nam, C.Y.; Sfeir, M.Y.; Black, C. Efficient organic solar cells with helical perylene diimide electron acceptors. *J. Am. Chem. Soc.* **2014**, *136*, 15215–15221. [CrossRef] [PubMed]
31. Pan, Q.-Q.; Li, S.-B.; Wu, Y.; Sun, G.-Y.; Geng, Y.; Su, Z.-M. A comparative study of a fluorene-based non-fullerene electron acceptor and pc61bm in an organic solar cell at a quantum chemical level. *RSC Adv.* **2016**, *6*, 81164–81173. [CrossRef]
32. Yan, C.Q.; Barlow, S.; Wang, Z.H.; Yan, H.; Jen, A.K.Y.; Marder, S.R.; Zhan, X.W. Non-fullerene acceptors for organic solar cells. *Nat. Rev. Mater.* **2018**, *3*, 19. [CrossRef]
33. Yuan, J.; Zhang, Y.; Zhou, L.; Zhang, G.; Yip, H.-L.; Lau, T.-K.; Lu, X.; Zhu, C.; Peng, H.; Johnson, P.A.; et al. Single-Junction organic solar cell with over 15% efficiency using fused-ring acceptor with electron-deficient core. *Joule* **2019**, *3*, 1140–1151. [CrossRef]
34. Li, R.; Liu, G.; Fan, B.; Du, X.; Tang, X.; Li, N.; Ying, L.; Brabec, C.J.; Huang, F.; Cao, Y. Non-fullerene acceptors end-capped with an extended conjugation group for efficient polymer solar cells. *Org. Electron.* **2018**, *59*, 366–373. [CrossRef]
35. Hohenberg, P.; Kohn, W. Inhomogeneous electron gas. *Phys. Rev.* **1964**, *136*, 864–871. [CrossRef]
36. Becke, A.D. Density-functional exchange-energy approximation with correct asymptotic behavior. *Phys. Rev. A* **1988**, *38*, 3098–3100. [CrossRef]
37. Tolbert, L.M. Solitons in a box: The organic chemistry of electrically conducting polyenes. *Acc. Chem. Res.* **1992**, *25*, 561–568. [CrossRef]
38. Perdew, J.P.; Burke, K.; Ernzerhof, M. Generalized gradient approximation made simple. *Phys. Rev. Lett.* **1998**, *77*, 3865–3868. [CrossRef]
39. Yanai, T.; Tew, D.P.; Handy, N.C. A new hybrid exchange-correlation functional using the Coulomb-attenuating method (CAM-B3LYP). *Chem. Phys. Lett.* **2004**, *393*, 51–57. [CrossRef]
40. Frisch, M.J.T.G.W.; Schlegel, H.B.; Scuseria, G.E.; Robb, M.A.; Cheeseman, J.R.S.G.; Barone, V.; Mennucci, B.; Petersson, G.A.N.H.; Caricato, M.; Li, X.; et al. *Gaussian 09*; Revision A.01; Gaussian Wallingford CT Inc.: Pittsburgh, PA, USA, 2009.
41. Kjellberg, P.; He, Z.; Pullerits, T. Bacteriochlorophyll in electric field. *J. Phys. Chem. B* **2003**, *107*, 13737–13742. [CrossRef]
42. Cave, R.J.; Newton, M.D. Calculation of electronic coupling matrix elements for ground and excited state electron transfer reactions: Comparison of the generalized Mulliken-Hush and block diagonalization methods. *J. Chem. Phys.* **1997**, *106*, 9213–9226. [CrossRef]

43. Lu, T.; Chen, F. Multiwfn: A multifunctional wavefunction analyzer. *J. Comput. Chem.* **2012**, *33*, 580–592. [CrossRef]
44. Marcus, R.A. Electron transfer reactions in chemistry: Theory and experiment (Nobel lecture). *Angew. Chem. Int. Ed. Engl.* **1993**, *32*, 1111–1121. [CrossRef]
45. Li, Y.F. Molecular design of photovoltaic materials for polymer solar cells: Toward suitable electronic energy levels and broad absorption. *Acc. Chem. Res.* **2012**, *45*, 723–733. [CrossRef] [PubMed]
46. Jhuo, H.J.; Yeh, P.N.; Liao, S.H.; Li, Y.L.; Cheng, Y.S.; Chen, S.A. Review on the Recent progress in low band gap conjugated polymers for bulk hetero-junction polymer solar cells. *J. Chin. Chem. Soc.* **2014**, *61*, 115–126. [CrossRef]
47. Yang, L.; Ren, A.M.; Feng, J.K.; Wang, J.F. Theoretical investigation of optical and electronic property modulations of pi-conjugated polymers based on the electron-rich 3,6-dimethoxy-fluorene unit. *J. Org. Chem.* **2005**, *70*, 3009–3020. [CrossRef]
48. Wang, L.; Li, T.; Shen, Y.; Song, Y. A theoretical study of the electronic structure and charge transport properties of thieno[2,3-b]benzothiophene based derivatives. *Phys. Chem. Chem. Phys.* **2016**, *18*, 8401–8411. [CrossRef] [PubMed]
49. Chattaraj, P.K.; Sarkar, U.; Roy, D.R. Electrophilicity index. *Chem. Rev.* **2006**, *106*, 2065–2091. [CrossRef] [PubMed]
50. Cheng, Y.; Qi, Y.; Tang, Y.; Zheng, C.; Wan, Y.; Huang, W.; Chen, R. Controlling intramolecular conformation through nonbonding interaction for soft-conjugated materials: Molecular design and optoelectronic properties. *J. Phys. Chem. Lett.* **2016**, *7*, 3609–3615. [CrossRef]
51. Zou, L.Y.; Ren, A.M.; Feng, J.K.; Liu, Y.L.; Ran, X.Q.; Sun, C.C. Theoretical Study on photophysical properties of multifunctional electroluminescent molecules with different π-conjugated bridges. *J. Phys. Chem. A* **2008**, *112*, 12172–12178. [CrossRef]
52. Kose, M.E.; Mitchell, W.J.; Kopidakis, N.; Chang, C.H.; Shaheen, S.E.; Kim, K.; Rumbles, G. Theoretical studies on conjugated phenyl-cored thiophene dendrimers for photovoltaic applications. *J. Am. Chem. Soc.* **2007**, *129*, 14257–14270. [CrossRef] [PubMed]
53. Janprapa, N.; Vchirawongkwin, V.; Kritayakornupong, C. Substituent effects on furan-phenylene copolymer for photovoltaic improvement: A density functional study. *Chem. Phys.* **2018**, *510*, 60–69. [CrossRef]
54. Shi, X.; Yang, Y.; Wang, L.; Li, Y. Introducing asymmetry induced by benzene substitution in a rigid fused π spacer of D-π-A-type solar cells: A computational investigation. *J. Phys. Chem. C* **2019**, *123*, 4007–4021. [CrossRef]
55. Ren, P.; Sun, C.; Shi, Y.; Song, P.; Yang, Y.; Li, Y. Global performance evaluation of solar cells using two models: From charge transfer and recombination mechanisms to photoelectric properties. *J. Mater. Chem. C* **2019**, *7*, 1934–1947. [CrossRef]
56. Ardo, S.; Meyer, G.J. Photodriven heterogeneous charge transfer with transition-metal compounds anchored to TiO2 semiconductor surfaces. *Chem. Soc. Rev.* **2009**, *38*, 115–164. [CrossRef] [PubMed]
57. Li, Y.; Xu, B.; Song, P.; Ma, F.; Sun, M. D-A-π-A System: Light harvesting, charge transfer, and molecular designing. *J. Phys. Chem. C* **2017**, *121*, 12546–12561. [CrossRef]
58. Belverdi, A.R.; Jamshidi, M.; Taherpour, A.; Jamshidi, M.; Rezaei, O. Novel donor-acceptor non-fullerene metal-organic solar cells: A first DFT and TD-DFT study. *Physica B* **2018**, *542*, 37–43. [CrossRef]
59. Pan, Q.Q.; Li, S.B.; Wu, Y.; Geng, Y.; Zhang, M.; Su, Z.M. Exploring more effective polymer donors for the famous non-fullerene acceptor ITIC in organic solar cells by increasing electron-withdrawing ability. *Org. Electron.* **2018**, *53*, 308–314. [CrossRef]
60. Cao, X.; Zhang, Q.; Zhou, K.; Yu, X.; Liu, J.; Han, Y.; Xie, Z. Improve exciton generation and dissociation by increasing fullerene content in the mixed phase of P3HT/fullerene. *Colloid Surf. A Physicochem. Eng. Asp.* **2016**, *506*, 723–731. [CrossRef]
61. Emelianova, E.V.; van der Auweraer, M.; Bassler, H. Hopping approach towards exciton dissociation in conjugated polymers. *J. Chem. Phys.* **2008**, *128*, 8. [CrossRef]
62. Marcus, R.A. Chemical and electrochemical electron-transfer theory. *Annu. Rev. Phys. Chem.* **1964**, *15*, 155–196. [CrossRef]
63. Song, P.; Li, Y.; Ma, F.; Pullerits, T.; Sun, M. Photoinduced electron transfer in organic solar cells. *Chem. Rec.* **2016**, *16*, 734–753. [CrossRef]

64. Voityuk, A.A. Estimation of electronic coupling in pi-stacked donor-bridge-acceptor systems: Correction of the two-state model. *J. Chem. Phys.* **2006**, *124*, 6. [CrossRef]
65. Song, P.; Li, Y.; Ma, F.; Pullerits, T.; Sun, M. External electric field-dependent photoinduced charge transfer in a donor-acceptor system for an organic solar cell. *J. Phys. Chem. C* **2013**, *117*, 15879–15889. [CrossRef]
66. Wen, K.K.; Pan, X.; Feng, S.Y.; Wu, W.P.; Guo, X.G.; Zhang, J.L. Theoretical design of azaacene-based non-fullerene electron transport material used in inverted perovskite solar cells. *Mol. Phys.* **2019**, *117*, 303–310. [CrossRef]
67. Bredas, J.L.; Beljonne, D.; Coropceanu, V.; Cornil, J. Charge-transfer and energy-transfer processes in pi-conjugated oligomers and polymers: A molecular picture. *Chem. Rev.* **2004**, *104*, 4971–5003. [CrossRef]
68. Leng, C.; Qin, H.; Si, Y.; Zhao, Y. Theoretical prediction of the rate constants for exciton dissociation and charge recombination to a triplet state in PCPDTBT with different fullerene derivatives. *J. Phys. Chem. C* **2014**, *118*, 1843–1855. [CrossRef]
69. Zhang, X.; Chi, L.; Ji, S.; Wu, Y.; Song, P.; Han, K.; Guo, H.; James, T.D.; Zhao, J. Rational design of d-PeT phenylethynylated-carbazole monoboronic acid fluorescent sensors for the selective detection of alpha-hydroxyl carboxylic acids and monosaccharides. *J. Am. Chem. Soc.* **2009**, *131*, 17452. [CrossRef]
70. Bredas, J.L.; Calbert, J.P.; da Silva Filho, D.A.; Cornil, J. Organic semiconductors: A theoretical characterization of the basic parameters governing charge transport. *Proc. Natl. Acad. Sci. USA* **2002**, *99*, 5804–5809. [CrossRef]
71. Lan, Y.K.; Huang, C.I. A theoretical study of the charge transfer behavior of the highly regioregular poly-3-hexylthiophene in the ordered state. *J. Phys. Chem. B* **2008**, *112*, 14857–14862. [CrossRef]
72. Mahmood, A.; Tang, A.L.; Wang, X.C.; Zhou, E.J. First-principles theoretical designing of planar non-fullerene small molecular acceptors for organic solar cells: Manipulation of noncovalent interactions. *Phys. Chem. Chem. Phys.* **2019**, *21*, 2128–2139. [CrossRef] [PubMed]
73. Yang, X.D.; Wang, L.J.; Wang, C.L.; Long, W.; Shuai, Z.G. Influences of crystal structures and molecular sizes on the charge mobility of organic semiconductors: Oligothiophenes. *Chem. Mater.* **2008**, *20*, 3205–3211. [CrossRef]
74. Deng, W.Q.; Goddard, W.A. Predictions of hole mobilities in oligoacene organic semiconductors from quantum mechanical calculations. *J. Phys. Chem. B* **2004**, *108*, 8614–8621. [CrossRef]
75. Coropceanu, V.; Cornil, J.; Silva Filho, D.A.D.; Olivier, Y.; Silbey, R.; Bredas, J.L. Charge transport in organic semiconductors. *Chem. Rev.* **2007**, *107*, 926–952. [CrossRef] [PubMed]
76. Blouin, N.; Michaud, A.; Gendron, D.; Wakim, S.; Blair, E.; Neagu-Plesu, R.; Belletete, M.; Durocher, G.; Tao, Y.; Leclerc, M. Toward a rational design of poly(2,7-carbazole) derivatives for solar cells. *J. Am. Chem. Soc.* **2008**, *130*, 732–742. [CrossRef] [PubMed]
77. Credgington, D.; Durrant, J.R. Insights from transient optoelectronic analyses on the open-circuit voltage of organic solar cells. *J. Phys. Chem. Lett.* **2012**, *3*, 1465–1478. [CrossRef] [PubMed]
78. Bijleveld, J.C.; Verstrijden, R.A.M.; Wienk, M.M.; Janssen, R.A.J. Maximizing the open-circuit voltage of polymer: Fullerene solar cells. *Appl. Phys. Lett.* **2010**, *97*, 181. [CrossRef]
79. Green, M.A. Solar cell fill factors: General graph and empirical expressions. *Solid-State Electron.* **1981**, *24*, 788–789. [CrossRef]
80. Zhang, L.; Shen, W.; He, R.; Liu, X.; Tang, X.; Yang, Y.; Li, M. Fine structural tuning of diketopyrrolopyrrole-cored donor materials for small molecule-fullerene organic solar cells: A theoretical study. *Org. Electron.* **2016**, *32*, 134–144. [CrossRef]
81. Liu, X.; Du, X.; Wang, J.; Duan, C.; Tang, X.; Heumueller, T.; Liu, G.; Li, Y.; Wang, Z.; Wang, J.; et al. Efficient organic solar cells with extremely high open-circuit voltages and low voltage losses by suppressing nonradiative recombination losses. *Adv. Energy Mater.* **2018**, *8*, 1801699. [CrossRef]
82. Boyuan, Q.; Jizheng, W. Fill factor in organic solar cells. *Phys. Chem. Chem. Phys.* **2013**, *15*, 8972–8982.
83. Scharber, M.C.; Mühlbacher, D.; Koppe, M.; Denk, P.; Waldauf, C.; Heeger, A.J.; Brabec, C.J. Design rules for donors in bulk-heterojunction solar cells-towards 10% energy-conversion efficiency. *Adv. Mater.* **2006**, *18*, 789–794. [CrossRef]
84. Dennler, G.; Scharber, M.C.; Brabec, C.J. Polymer-fullerene bulk-heterojunction solar cells. *Adv. Mater.* **2009**, *21*, 1323–1338. [CrossRef]

85. Lashkari, M.; Arshadi, M.R. DFT studies of pyridine corrosion inhibitors in electrical double layer: Solvent, substrate, and electric field effects. *Chem. Phys.* **2004**, *299*, 131–137. [CrossRef]
86. Ferrighi, L.; Frediani, L.; Cappelli, C.; Sałek, P.; Ågren, H.; Helgaker, T.; Ruud, K. Density-functional-theory study of the electric-field-induced second harmonic generation (EFISHG) of push–pull phenylpolyenes in solution. *Chem. Phys. Lett.* **2006**, *425*, 267–272. [CrossRef]

© 2019 by the authors. Licensee MDPI, Basel, Switzerland. This article is an open access article distributed under the terms and conditions of the Creative Commons Attribution (CC BY) license (http://creativecommons.org/licenses/by/4.0/).